CHEMISTRY OF MATERIALS

Communication

pubs.acs.org/cm

Tuning *p*-Type Transport in Bottom-Up-Engineered Nanocrystalline Pb Chalcogenides Using Alkali Metal Chalcogenides as Capping Ligands

Maria Ibáñez,[†,‡] Roger Hasler,[†,‡] Yu Liu,[§] Oleksandr Dobrozhan,[§] Olga Nazarenko,[†,‡] Doris Cadavid,[§] Andreu Cabot,[§,#] and Maksym V. Kovalenko*[,†,‡]

[†]Institute of Inorganic Chemistry, Department of Chemistry and Applied Biosciences, ETH Zürich, Vladimir Prelog Weg 1, Zürich CH-8093, Switzerland

[‡]Empa-Swiss Federal Laboratories for Materials Science and Technology, Überlandstrasse 129, Dübendorf CH-8600, Switzerland

[§]Catalonia Energy Research Institute - IREC, Sant Adria del Besos, 08930 Barcelona, Spain

[#]ICREA, Pg. Lluís Company 23, 08010 Barcelona, Spain

Supporting Information

Colloidally synthesized nanocrystals (NCs) are presently employed as artificial atoms for predictable design of solid-state materials for a plethora of applications.[1,2] Tuning the electronic characteristics, foremost type, concentration and mobility of charge carriers remains a formidable challenge for bottom-up engineered nanostructures. As-synthesized NCs are usually capped with long-chain organic ligands covalently attached to surface NC atoms.[3] These ligands hamper electronic transport in NC-based materials, making the removal of these electrically insulating shells absolutely necessary. Organic ligands are often replaced by strongly or weakly coordinating, shorter, organic or inorganic ligands such as pyridine,[4] hydrazine,[5] ammonia,[6] thiols,[7] chalcogenidometalates,[8,9] thiocyanate,[10,11] tetrafluoroborate salts,[12] oxometalates,[13] halides,[14] halometalates[15] or chalcogenides,[16−18] metal ions,[19,20] etc. The capping of NCs with such ligands enhances electronic coupling between adjacent NCs and allows for the modulation of nearly all practically relevant electronic parameters.[21,22]

Similar to bulk semiconductors, intrinsic stoichiometry and extrinsic impurities can be expected as primary players for controlling *n*-, *p*- or intrinsic charge transport (Scheme 1). The combined effect of the NC core composition and of the chosen capping ligand can be rationalized considering charge-orbital balance.[25] In the case of NCs, charge and bond counting must also include covalently attached ligands and/or surface charges. In particular, colloidal NCs of lead chalcogenides (PbX, X = S, Se, Te) contain a fully stoichiometric core covered with an excess of Pb cations, acting as adatoms for coordinating with X-type capping ligands such as carboxylates.[26] The fate of this additional quantity of Pb must be considered for controlling and understanding the electronic properties of the final solid material, as discussed later for various surface treatments. Extrinsic dopants for substitutional doping can be introduced via surface functionalization. Surface passivation with halide ions (Cl^-, Br^- and I^-) has been shown to result in NC solids with *n*-type conductivity with adjustable charge carrier mobility and concentration.[23,27] This *n*-type doping effect from halide ions can be rationalized based on the charge neutrality requirement: substitution of one double-charged chalcogenide anion with a single-charged halide ion and an electron, as illustrated in Scheme 1.

Analogously, an efficient *p*-type doping strategy is to replace a double-charged Pb or Sn ion with a single-charged cation, such as potassium or sodium, and a hole (Scheme 1). For accomplishing this with colloidal PbS NCs as starting building blocks, a two-step strategy is detailed. First, an alkali metal containing inorganic capping ligand (K_2S, K_2Te and Na_2S) is attached to the surface via a ligand-exchange reaction. Second, substitutional doping is induced by thermal annealing. We then thoroughly characterize the charge transport by electrical conductivity (σ), Hall-effect and thermopower (Seebeck coefficient, S) measurements. A variety of control experiments with other ligands, for differentiating the effects of chalcogen and alkali metals, is presented. Experimental results show that tunable *p*-type conductivity can be accomplished with various NC−ligand combinations, either chalcogen-matched (i.e., PbS-K_2S) or mismatched (i.e., PbS-K_2Te). Furthermore, fine-tuning of hole concentration has been demonstrated with a mixture of ligands, wherein one contains alkali metal (e.g., A_2X) and the

Scheme 1. Atomic Depiction of Substitutional Electronic Doping for Rendering PbS *n*-Type[23] or *p*-Type (this work) with High Carrier Density[a]

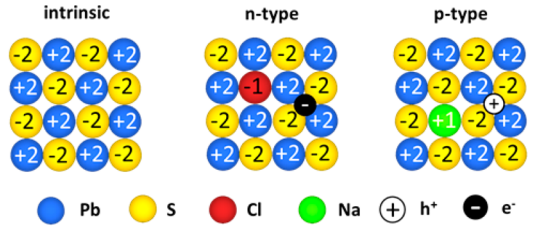

[a]The similarity in corresponding Shannon ionic radii[24] of cations (133 pm for Pb^{2+} and 116 pm for Na^+) and anions (184 pm for S^{2-} and 181 pm for Cl^-) favors high doping levels.

Received: July 17, 2017
Revised: August 20, 2017
Published: August 23, 2017

DOI: 10.1021/acs.chemmater.7b02967
Chem. Mater. 2017, 29, 7093−7097

other contains only the chalcogen (X dissolved in a dithiol/diamine mixture; denoted as X-complexes).

In the following, the details of the surface functionalization and resulting electronic properties are presented for ~11 nm cubic PbS NCs for seven ligands and their mixtures, to illustrate the rational chemical engineering of *p*-type conductivity in nanostructured Pb chalcogenides (Figure 1). All samples differ

a)

Surface treatment	Carrier concentration (cm^{-3})	Carrier mobility ($cm^{-3}\ V^{-1}s^{-1}$)	Electrical conductivity ($S\ cm^{-1}$)	Seebeck coefficient ($\mu V\ K^{-1}$)
OA (■)	p= 1 x 10^{16}	43	0.07	398
N_2H_4 (▲)	n= 2 x 10^{19}	6	20	-202
S-complexes (●)	n= 8 x 10^{17}	23	3	-129
K_2S (◆)	p= 2 x 10^{16}	138	0.2	435
0.05S:0.95Na_2S (◄)	p= 1 x 10^{17}	43	1.4	294
0.10S:0.90Na_2S (►)	p= 5 x 10^{17}	37	2.7	202
Na_2S (●)	p= 9 x 10^{17}	34	5	129

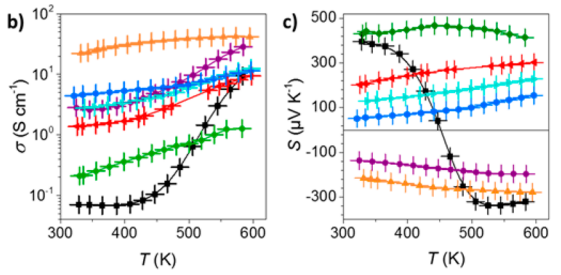

Figure 1. (a) Summary of the used ligands for the surface functionalization/treatment of 11 nm PbS NCs and resulting transport properties at RT. (b) Temperature-dependent electrical conductivities, σ. (c) Temperature dependence of the Seebeck coefficients, S.

only in their surface treatment, whereas the temperatures and procedures of thermal consolidation are maintained very similarly (400–450 °C, see the Supporting Information (SI) for further details on all synthesis procedures and characterizations, including Figures S1–S16 and Tables S1–S3).

To understand the intrinsic nature of the PbS NC and its relationship to the electronic properties of the corresponding nanomaterial, taking into account the purely inorganic part and the organic shell surrounding it, two reference samples were prepared. In the first reference, both inorganic core and organic shell were treated as a unit (OA-PbS). In a typical experiment, several grams of PbS NCs were prepared according to reported methods by reacting lead oleate with an oleylamine-based sulfur precursor.[23] Purified NCs were capped exclusively with long-chain oleate ligands, as confirmed by NMR measurements. Prior to the consolidation, such organic ligands were thermally decomposed by annealing the as-synthesized NCs at 450 °C under inert gas. The obtained powder was consolidated by hot-pressing into ~1 mm thick disk-shaped pellets, 10 mm in diameter (40 MPa, 420–440 °C, 4 min). Pellets obtained from oleate-capped PbS NCs (OA-PbS) exhibit low densities (~80%) attributed to decomposition and removal of the capping ligands.[28] Consequently, impurities of PbO and carbon, both quantities scaling with NC size (surface-to-volume ratio), are typically observed in such samples. These impurities accumulate at the grain boundaries.[29] For 11 nm PbS NCs, the amount of Pb-adatoms that are converted into PbO is estimated to be ca. 7.7 at. % of the stoichiometric core PbS (Tables S1 and S2). This material exhibits rather low room temperature (RT) electrical conductivities (0.07 S cm^{-1}, Figure 1b). A positive sign on the Seebeck coefficient (Figure 1c) indicates a *p*-type conductivity. Measurements of the Hall hole concentration at RT showed a relatively low doping level (p = 10^{16} cm^{-3}). As the temperature increased, thermally activated electrons increasingly contributed to the conductivity, as commonly observed for Pb chalcogenide solids,[6,23,30] eventually inverting the sign of the Seebeck coefficient to negative at ca. 450 K.

On the other hand, to evaluate the sole influence of the inorganic part of NCs, we have studied the case of a ligand-free surface design. Native organic ligands were removed using a 4 M solution of hydrazine in anhydrous ethanol. Ethanol is known to desorb oleate from the NC surface through the nucleophilic addition of ethoxide to the carboxylate group, which activates the protonation of the oleate and consequently its desorption.[31] In the presence of hydrazine, the concentration of ethoxide nucleophiles increases promoting oleate removal and generating desorbed oleic acid and oleic hydrazide.[31] Additionally, hydrazine was selected due to its strong reducing character, which allows for producing non-oxidized, fully inorganic compositions, without introducing new chemical elements into consideration.[32,33] Solids produced from N_2H_4-treated PbS NCs exhibited high electrical conductivities and a negative Seebeck coefficient in the whole temperature range. Hall electron concentrations, measured at RT, were on the order of 2 × 10^{19} cm^{-3}, much higher than that of the OA-PbS-derived nanomaterial. This can be ascribed to the conversion of divalent Pb-adatoms to Pb^0, acting as *n*-type dopants.[34,35]

Surface modification with K_2S, K_2Te and Na_2S was carried out via a phase-transfer reaction, in which the PbS NCs migrated from the nonpolar phase (hexane) to the polar phase (*N*-methylformamide; MFA) upon displacement of oleate ligands with the alkali metal chalcogenides (Figure 2a, Figure S16). MFA was chosen due to its high dielectric constant, which facilitates the electrostatic dissociation of the alkali counterions and the adsorption of anionic ligands onto the NC

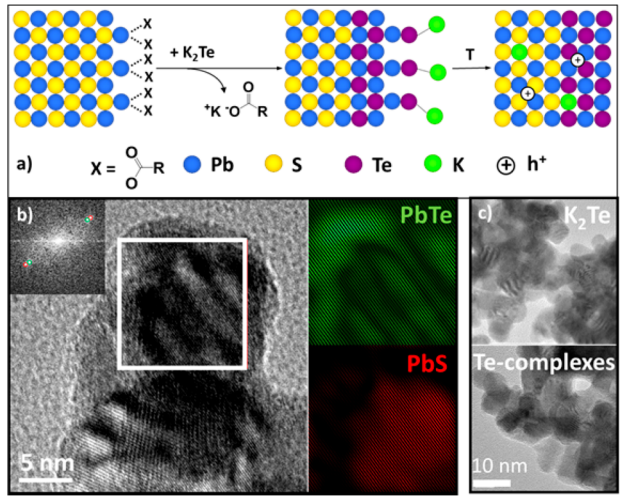

Figure 2. (a) Schematic of the ligand-exchange reaction at the surface of PbS NCs: oleate ions are replaced with Te^{2-}; partial S^{2-}-to-Te^{2-} anion exchange also occurs. K-ions occupy Pb sites in the final solid. (b) HRTEM images after the surface treatment with K_2Te for 17 h, displaying Moiré fringers and crystallographic maps showing the core–shell PbS@PbTe structure. (c) Lower resolution TEM images after treatment with K_2Te (top) and Te-complexes (bottom) for 17 h.

DOI: 10.1021/acs.chemmater.7b02967
Chem. Mater. 2017, 29, 7093–7097

surface. Consequently, the steric stabilization of NC colloids is switched to electrostatic stabilization (Figure S4). A byproduct of alkali metal oleate was fully removed by several cycles of precipitation and redispersion of NCs in MFA, using acetone as a nonsolvent to cause precipitation. An analogous phase-transfer approach was utilized in order to treat PbS NCs with molecular chalcogen complexes (X-complexes). The latter were prepared by dissolving ~4 wt % of elemental chalcogens in ethanedithiol−ethylenediamine (1:4) mixtures.[36] In the subsequent ligand-exchange process, the polar phase was composed of an MFA:ethylenediamine (1:1) mixture, and acetone was replaced with acetonitrile as a nonsolvent. For a controlled introduction of varying quantities of alkali metals onto the NC surface, A_2X ligands and X-complexes can be mixed in desired ratios.

The functionalization of initially Pb-rich PbS NCs with S-complexes, followed by thermal consolidation is assumed to yield PbS nanomaterial with a stoichiometry closer to 1:1, similar to the reported effect of the ammonium thiocyanate ligand.[23] The oxidation state of the Pb-adatoms should rather follow the N_2H_4-scenario (*n*-type), but the quantity of the formed Pb^0 should be much lower, if any. In accordance with these considerations, this nanomaterial indeed shows a negative Seebeck coefficient in the whole temperature range, with carrier concentrations ($n = 8 \times 10^{17}$ cm^{-3}) 25 times lower than in the case of N_2H_4-treatment, but much higher than for OA-PbS. Similarly, bulk PbS had been shown to acquire *n*-type conductivity due to a slight Pb surplus, caused by the S loss upon prolonged annealing.[37]

In striking contrast to a previous example, solids derived from A_2S-treated (A = K, Na) PbS NCs (Figure 1) exhibited clear *p*-type behavior, apparent from the positive sign of the Seebeck coefficients in the whole temperature range. The Hall hole concentrations in Na_2S−PbS and K_2S−PbS nanomaterials, measured at RT, were $p = 9 \times 10^{17}$ cm^{-3} and $p = 2 \times 10^{16}$ cm^{-3}, respectively. This is consistent with the doping scenario depicted in Scheme 1: Pb surplus at the surface is neutralized by additional chalcogenide anions from the ligand, and some Pb ions are substituted with shallow electron acceptors (A^+) incorporated into the cation sublattice. In other words, Pb^{2+} is substituted by a localized K^+ (or Na^+) and a mobile hole (h^+). The highest achievable hole concentrations were ca. 9×10^{17} cm^{-3} (at RT). The difficulty of reaching even higher hole concentrations in this bottom-up approach is attributed to the deficiency of S, counteracting the *p*-doping from alkali metals.

To overcome the doping limitation inherent to S-based nanomaterial we investigated Te-based ligands. The amount of chalcogen-based ligand used in the ligand-exchange reaction is always much higher than that required for binding each Pb-adatom at the NC surface. Hence, the observation of core−shell PbS@PbTe NCs (Figure 2) is unsurprising, caused by the anion-exchange occurring when PbS NCs were subjected to Te-based ligands. High-resolution transmission electron microscopy (HRTEM) micrographs of the produced PbS@PbTe NCs revealed the presence of Moiré fringes characteristic of the superposition of different crystal phases. The doublet points marked by red and green in the power spectrum allowed for differentiation between the core and the shell lattice. Both core and shell have identical cubic rock-salt crystal structure (S.G.: *Fm*3*m*) and differ only in the lattice constant (6.46 and 5.94 Å for PbTe and PbS, respectively). Low-magnification images revealed that the formation of PbTe during ligand removal induced NC sintering through the PbTe shell (Figure 2c). Both the duration of the ligand exchange in solution (up to 500 h) and thermal treatment (10 min, 210 °C) contribute to the degree of the anion-exchange and crystallinity of the produced PbTe shells. The resulting powder X-ray diffraction (XRD) pattern indicates that the anion-exchange occurs rapidly in solution within seconds (Figure 3, S8). Longer reaction times

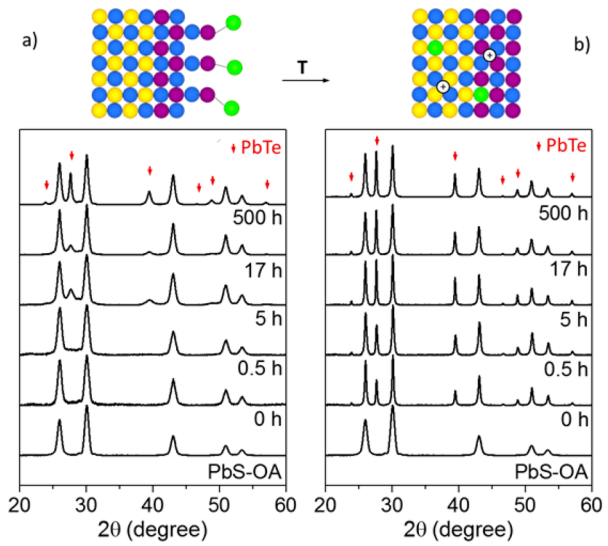

Figure 3. XRD patterns of PbS NCs after the exchange of oleate with K_2Te recorded for different ligand-exchange reaction times before (a) and after (b) annealing at 210 °C. Color code for atoms is same as in Figure 2.

lead to crystallization of PbTe already at RT. PbTe content increases only slightly from 23% after 0.5 h to 30% after 500 h (as determined from Rietveld refinement).

Such Te-ion-exchanged PbS NCs, using K_2Te or Te-complexes, were thermally consolidated by hot-pressing into solids of the approximate composition $K_{0.01}Pb_{0.99}S_{0.7}Te_{0.3}$ (denoted as K_2Te-PbS) and $PbS_{0.7}Te_{0.3}$ (i.e., Te-PbS). K_2Te-PbS nanocomposites exhibited strong *p*-type behavior, with high electrical conductivities over the whole studied temperature range, Hall hole concentrations of approximately 3×10^{19} cm^{-3} at RT, and a positive sign and value of 222 μV K^{-1} for the Seebeck coefficient (Figure 4). In contrast, in the case of Te−PbS nanocomposites, much lower electrical conductivities and low carrier concentrations were obtained ($p = 10^{16}$ cm^{-3}), indicating a quasi-intrinsic behavior (very low doping levels). Seebeck coefficients were also much smaller (103 μV K^{-1}) with a sign inversion at approximately 470 K; a behavior associated with bipolar effects. At RT, electronic transport was somewhat dominated by holes, and as the temperature increased, the electrons become the major carrier type. Carrier concentration could be further tuned in the range of 10^{16}−10^{19} cm^{-3} by combining K_2Te- and Te-treated NCs in various ratios (Figure 4).

The approach presented herein, which combines surface functionalization and thermally induced substitutional doping, can be extended to other semiconductor NCs. As an example, in a fully lead-free system, derived in an analogous manner from colloidal SnSe NCs and K_2Se as capping ligands, a *p*-type electrical transport with Seebeck coefficients of 320 μV K^{-1} and high hole concentrations of 6×10^{17} cm^{-3} were obtained at RT (Figure 5).

DOI: 10.1021/acs.chemmater.7b02967
Chem. Mater. 2017, 29, 7093−7097

a)

Surface treatment	Carrier concentration (cm^{-3})	Carrier mobility ($cm^{-3}\ V^{-1}s^{-1}$)	Electrical conductivity ($S\ cm^{-1}$)	Seebeck coefficient ($\mu V\ K^{-1}$)
OA (■)	n= 2 x 10^{17}	3	0.1	-90
Te-complexes (▼)	p= 1 x 10^{16}	312	0.5	103
K_2Te (►)	p= 3 x 10^{19}	9	41.4	222
0.05Te:0.95K_2Te (●)	p= 1 x 10^{19}	11	17.7	336
0.10Te:0.90K_2Te (◄)	p= 7 x 10^{18}	2	2.5	278

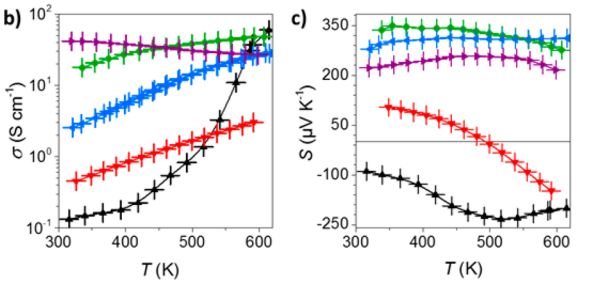

Figure 4. (a) Summary of the results obtained with Te-based ligands and 11 nm PbS NCs at RT. (b) Temperature-dependent electrical conductivities and (c) Seebeck coefficients.

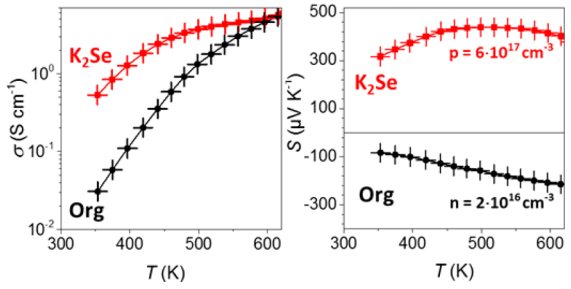

Figure 5. Temperature-dependent electrical conductivity (left) and Seebeck coefficient (right) of SnSe nanocomposites obtained from organic-capped and K_2Se-treated SnSe NCs.

In summary, a bottom-up strategy to produce fully inorganic, nanostructured Pb chalcogenide solids with tunable *p*-type transport using colloidal PbS NCs as initial building blocks has been presented. In particular, surface functionalization was used as a platform to modulate NC stoichiometry as well as to introduce controlled amounts of dopants. Substitutional doping with K^+ and Na^+ ions, with hole concentrations adjustable up to 3×10^{19} cm^{-3}, was accomplished via ligand exchange of the native organic surface molecules with alkali metal chalcogenides, followed by thermal consolidation into densely packed solids. We envision this strategy to be highly instrumental for both thin-film and bulk-like solids, with possible applications in thermoelectrics and electronics.

■ ASSOCIATED CONTENT

Supporting Information

The Supporting Information is available free of charge on the ACS Publications website at DOI: 10.1021/acs.chemmater.7b02967.

Details of the chemicals used, NCs syntheses; ligand exchange reactions; pellet fabrication, materials characterization (nuclear magnetic resonance spectra, X-ray diffraction patterns, thermogravimetry measurements, inductively coupled plasma mass spectrometry results); charge transport measurements, and additional notes (PDF)

■ AUTHOR INFORMATION

Corresponding Author

*M. V. Kovalenko. E-mail: mvkovalenko@ethz.ch.

ORCID

Maria Ibáñez: 0000-0001-5013-2843
Andreu Cabot: 0000-0002-7533-3251
Maksym V. Kovalenko: 0000-0002-6396-8938

Notes

The authors declare no competing financial interest.

■ ACKNOWLEDGMENTS

This work was financially supported by the European Union (EU) via FP7 ERC Starting Grant 2012 (Project NANOSOLID, GA No. 306733). M.I. was supported by AGAUR via Beatriu i Pinós fellowship and by ETH Zurich via ETH career seed grant (SEED-18 16-2). IREC acknowledges funding from Generalitat de Catalunya (2014SGR1638).

■ REFERENCES

(1) Kovalenko, M. V.; Manna, L.; Cabot, A.; Hens, Z.; Talapin, D. V.; Kagan, C. R.; Klimov, V. I.; Rogach, A. L.; Reiss, P.; Milliron, D. J.; Guyot-Sionnnest, P.; Konstantatos, G.; Parak, W. J.; Hyeon, T.; Korgel, B. A.; Murray, C. B.; Heiss, W. Prospects of Nanoscience with Nanocrystals. *ACS Nano* **2015**, *9*, 1012−1057.

(2) Ortega, S.; Ibáñez, M.; Liu, Y.; Zhang, Y.; Kovalenko, M. V.; Cadavid, D.; Cabot, A. Bottom-Up Engineering of Thermoelectric Nanomaterials and Devices from Solution-Processed Nanoparticle Building Blocks. *Chem. Soc. Rev.* **2017**, *46*, 3510−3528.

(3) De Roo, J.; De Keukeleere, K.; Hens, Z.; Van Driessche, I. From Ligands to Binding Motifs and Beyond; the Enhanced Versatility of Nanocrystal Surfaces. *Dalton Trans.* **2016**, *45*, 13277−13283.

(4) Gur, I.; Fromer, N. A.; Geier, M. L.; Alivisatos, A. P. Air-Stable All-Inorganic Nanocrystal Solar Cells Processed from Solution. *Science* **2005**, *310*, 462−465.

(5) Fang, H.; Yang, H.; Wu, Y. Thermoelectric Properties of Silver Telluride−Bismuth Telluride Nanowire Heterostructure Synthesized by Site-Selective Conversion. *Chem. Mater.* **2014**, *26*, 3322−3327.

(6) Scheele, M.; Oeschler, N.; Veremchuk, I.; Peters, S.-O.; Littig, A.; Kornowski, A.; Klinke, C.; Weller, H. Thermoelectric Properties of Lead Chalcogenide Core−Shell Nanostructures. *ACS Nano* **2011**, *5*, 8541−8551.

(7) Leschkies, K. S.; Beatty, T. J.; Kang, M. S.; Norris, D. J.; Aydil, E. S. Solar Cells Based on Junctions between Colloidal PbSe Nanocrystals and Thin ZnO Films. *ACS Nano* **2009**, *3*, 3638−3648.

(8) Kovalenko, M. V.; Scheele, M.; Talapin, D. V. Colloidal Nanocrystals with Molecular Metal Chalcogenide Surface Ligands. *Science* **2009**, *324*, 1417−1420.

(9) Buckley, J. J.; Greaney, M. J.; Brutchey, R. L. Ligand Exchange of Colloidal CdSe Nanocrystals with Stibanates Derived from Sb_2S_3 Dissolved in a Thiol-Amine Mixture. *Chem. Mater.* **2014**, *26*, 6311−6317.

(10) Fafarman, A. T.; Koh, W.-k.; Diroll, B. T.; Kim, D. K.; Ko, D.-K.; Oh, S. J.; Ye, X.; Doan-Nguyen, V.; Crump, M. R.; Reifsnyder, D. C.; Murray, C. B.; Kagan, C. R. Thiocyanate-Capped Nanocrystal Colloids: Vibrational Reporter of Surface Chemistry and Solution-Based Route to Enhanced Coupling in Nanocrystal Solids. *J. Am. Chem. Soc.* **2011**, *133*, 15753−15761.

(11) Koh, W.-k.; Saudari, S. R.; Fafarman, A. T.; Kagan, C. R.; Murray, C. B. Thiocyanate-Capped PbS Nanocubes: Ambipolar Transport Enables Quantum Dot Based Circuits on a Flexible Substrate. *Nano Lett.* **2011**, *11*, 4764−4767.

(12) Dong, A.; Ye, X.; Chen, J.; Kang, Y.; Gordon, T.; Kikkawa, J. M.; Murray, C. B. A Generalized Ligand-Exchange Strategy Enabling Sequential Surface Functionalization of Colloidal Nanocrystals. *J. Am. Chem. Soc.* **2011**, *133*, 998−1006.

DOI: 10.1021/acs.chemmater.7b02967
Chem. Mater. 2017, 29, 7093−7097

(13) Huang, J.; Liu, W.; Dolzhnikov, D. S.; Protesescu, L.; Kovalenko, M. V.; Koo, B.; Chattopadhyay, S.; Shenchenko, E. V.; Talapin, D. V. Surface Functionalization of Semiconductor and Oxide Nanocrystals with Small Inorganic Oxoanions (PO_4^{3-}, MoO_4^{2-}) and Polyoxometalate Ligands. *ACS Nano* **2014**, *8*, 9388−9402.
(14) Tang, J.; Kemp, K. W.; Hoogland, S.; Jeong, K. S.; Liu, H.; Levina, L.; Furukawa, M.; Wang, X.; Debnath, R.; Cha, D.; Chou, K. W.; Fischer, A.; Amassian, A.; Asbury, J. B.; Sargent, E. H. Colloidal-Quantum-Dot Photovoltaics Using Atomic-Ligand Passivation. *Nat. Mater.* **2011**, *10*, 765−771.
(15) Dirin, D. N.; Dreyfuss, S.; Bodnarchuk, M. I.; Nedelcu, G.; Papagiorgis, P.; Itskos, G.; Kovalenko, M. V. Lead Halide Perovskites and Other Metal Halide Complexes As Inorganic Capping Ligands for Colloidal Nanocrystals. *J. Am. Chem. Soc.* **2014**, *136*, 6550−6553.
(16) Nag, A.; Kovalenko, M. V.; Lee, J.-S.; Liu, W.; Spokoyny, B.; Talapin, D. V. Metal-free Inorganic Ligands for Colloidal Nanocrystals: S^{2-}, HS^-, Se^{2-}, HSe^-, Te^{2-}, HTe^-, TeS_3^{2-}, OH^-, and NH^{2-} as Surface Ligands. *J. Am. Chem. Soc.* **2011**, *133*, 10612−10620.
(17) Otto, T.; Miller, C.; Tolentino, J.; Liu, Y.; Law, M.; Yu, D. Gate-Dependent Carrier Diffusion Length in Lead Selenide Quantum Dot Field-Effect Transistors. *Nano Lett.* **2013**, *13*, 3463−3469.
(18) Shanker, G. S.; Swarnkar, A.; Chatterjee, A.; Chakraborty, S.; Phukan, M.; Parveen, N.; Biswas, K.; Nag, A. Electronic grade and flexible semiconductor film employing oriented attachment of colloidal ligand-free PbS and PbSe nanocrystals at room temperature. *Nanoscale* **2015**, *7*, 9204−9214.
(19) Cadavid, D.; Ibáñez, M.; Shavel, A.; Dura, O. J.; Lopez de la Torre, M. A.; Cabot, A. Organic Ligand Displacement by Metal Salts to Enhance Nanoparticle Functionality: Thermoelectric Properties of Ag_2Te. *J. Mater. Chem. A* **2013**, *1*, 4864−4870.
(20) Nag, A.; Chung, D. S.; Dolzhnikov, D. S.; Dimitrijevic, N. M.; Chattopadhyay, S.; Shibata, T.; Talapin, D. V. Effect of Metal Ions on Photoluminescence, Charge Transport, Magnetic and Catalytic Properties of All-Inorganic Colloidal Nanocrystals and Nanocrystal Solids. *J. Am. Chem. Soc.* **2012**, *134*, 13604−13615.
(21) Stavrinadis, A.; Konstantatos, G. Strategies for the Controlled Electronic Doping of Colloidal Quantum Dot Solids. *ChemPhysChem* **2016**, *17*, 632−644.
(22) Liu, Y.; Gibbs, M.; Puthussery, J.; Gaik, S.; Ihly, R.; Hillhouse, H. W.; Law, M. Dependence of Carrier Mobility on Nanocrystal Size and Ligand Length in PbSe Nanocrystal Solids. *Nano Lett.* **2010**, *10*, 1960−1969.
(23) Ibáñez, M.; Korkosz, R. J.; Luo, Z.; Riba, P.; Cadavid, D.; Ortega, S.; Cabot, A.; Kanatzidis, M. G. Electron Doping in Bottom-Up Engineered Thermoelectric Nanomaterials through HCl-Mediated Ligand Displacement. *J. Am. Chem. Soc.* **2015**, *137*, 4046−4049.
(24) Shannon, R. Revised Effective Ionic Radii and Systematic Studies of Interatomic Distances in Halides and Chalcogenides. *Acta Crystallogr., Sect. A: Cryst. Phys., Diffr., Theor. Gen. Crystallogr.* **1976**, *32*, 751−767.
(25) Voznyy, O.; Zhitomirsky, D.; Stadler, P.; Ning, Z.; Hoogland, S.; Sargent, E. H. A Charge-Orbital Balance Picture of Doping in Colloidal Quantum Dot Solids. *ACS Nano* **2012**, *6*, 8448−8455.
(26) Moreels, I.; Fritzinger, B.; Martins, J. C.; Hens, Z. Surface Chemistry of Colloidal PbSe Nanocrystals. *J. Am. Chem. Soc.* **2008**, *130*, 15081−15086.
(27) Zhitomirsky, D.; Furukawa, M.; Tang, J.; Stadler, P.; Hoogland, S.; Voznyy, O.; Liu, H.; Sargent, E. H. N-Type Colloidal-Quantum-Dot Solids for Photovoltaics. *Adv. Mater.* **2012**, *24*, 6181−6185.
(28) Marks, B. M.; Howard, H. C. The Catalytic Decomposition of Oleic Acid. *J. Phys. Chem.* **1927**, *32*, 1040−1048.
(29) Ibáñez, M.; Luo, Z.; Genc, A.; Piveteau, L.; Ortega, S.; Cadavid, D.; Dobrozhan, O.; Liu, Y.; Nachtegaal, M.; Zebarjadi, M.; Arbiol, J.; Kovalenko, M. V.; Cabot, A. High-Performance Thermoelectric Nanocomposites from Nanocrystal Building Blocks. *Nat. Commun.* **2016**, *7*, 10766.
(30) Ibáñez, M.; Zamani, R.; Gorsse, S.; Fan, J.; Ortega, S.; Cadavid, D.; Morante, J. R.; Arbiol, J.; Cabot, A. Core-Shell Nanoparticles As Building Blocks for the Bottom-Up Production of Functional Nanocomposites: PbTe-PbS Thermoelectric Properties. *ACS Nano* **2013**, *7*, 2573−2586.
(31) Law, M.; Luther, J. M.; Song, Q.; Hughes, B. K.; Perkins, C. L.; Nozik, A. J. Structural, Optical, and Electrical Properties of PbSe Nanocrystal Solids Treated Thermally or with Simple Amines. *J. Am. Chem. Soc.* **2008**, *130*, 5974−5985.
(32) Ocier, C. R.; Whitham, K.; Hanrath, T.; Robinson, R. D. Chalcogenidometallate Clusters as Surface Ligands for PbSe Nanocrystal Field-Effect Transistors. *J. Phys. Chem. C* **2014**, *118*, 3377−3385.
(33) Scheele, M.; Oeschler, N.; Meier, K.; Kornowski, A.; Klinke, C.; Weller, H. Synthesis and Thermoelectric Characterization of Bi_2Te_3 Nanoparticles. *Adv. Funct. Mater.* **2009**, *19*, 3476−3483.
(34) Luther, J. M.; Pietryga, J. M. Stoichiometry Control in Quantum Dots: A Viable Analog to Impurity Doping of Bulk Materials. *ACS Nano* **2013**, *7*, 1845−1849.
(35) Oh, S. J.; Berry, N. E.; Choi, J.-H.; Gaulding, E. A.; Paik, T.; Hong, S.-H.; Murray, C. B.; Kagan, C. R. Stoichiometric Control of Lead Chalcogenide Nanocrystal Solids to Enhance Their Electronic and Optoelectronic Device Performance. *ACS Nano* **2013**, *7*, 2413−2421.
(36) Webber, D. H.; Buckley, J. J.; Antunez, P. D.; Brutchey, R. L. Facile Dissolution of Selenium and Tellurium in a Thiol-Amine Solvent Mixture under Ambient Conditions. *Chem. Sci.* **2014**, *5*, 2498−2502.
(37) Zhao, L.-D.; He, J.; Wu, C.-I.; Hogan, T. P.; Zhou, X.; Uher, C.; Dravid, V. P.; Kanatzidis, M. G. Thermoelectrics with Earth Abundant Elements: High Performance p-type PbS Nanostructured with SrS and CaS. *J. Am. Chem. Soc.* **2012**, *134*, 7902−7912.

DOI: 10.1021/acs.chemmater.7b02967
Chem. Mater. 2017, 29, 7093−7097